

# Supporting Information

## Effects of a Solid Solution Outer Layer of $\text{TiO}_2$ on the Surface and Electrochemical Properties of $\text{LiNi}_{0.6}\text{Co}_{0.2}\text{Mn}_{0.2}\text{O}_2$ Cathodes for Lithium-ion Batteries Through the Use of Thin-film Electrodes

*Wencong Wang<sup>†</sup>, Changhee Lee<sup>†</sup>, Danni Yu<sup>†</sup>, Yasuyuki Kondo<sup>‡</sup>, Yuto Miyahara<sup>†</sup>,  
Takeshi Abe<sup>†</sup>, and Kohei Miyazaki<sup>†\*</sup>*

<sup>†</sup> Graduate School of Engineering, Kyoto University, Nishikyo-ku, Kyoto, 615-8510,  
Japan

<sup>‡</sup> The Institute of Scientific and Industrial Research, Osaka University, Mihogaoka,  
Ibaraki, 567-0047, Osaka, Japan

\* Corresponding author

E-mail address: [myzkohei@elech.kuic.kyoto-u.ac.jp](mailto:myzkohei@elech.kuic.kyoto-u.ac.jp) (Kohei Miyazaki)

## S1. Additional Results and Discussion

### S1.1. Potential and temperature dependence of charge transfer resistances of NCM622-bare and NCM622-SSOL thin-film electrodes for $E_a$ calculation

EIS of the thin-films was measured to analyze the effects of the SSOL phase the electrochemical interfacial reaction of NCM622 thin-film electrodes. Figure S7 shows the potential dependence of charge transfer resistance ( $R_{ct}$ ) of the NCM622-bare thin-film electrode during the first cycle. In Nyquist plots, none of the semi-circle in the middle-low frequency region is recognized until the potential reached the oxidation position (3.70 V). Thus, the newly formed semi-circle observed above 3.70 V can be attributed to the  $R_{ct}$  at the interface between the thin-film electrode and electrolyte. In addition, the values of  $R_{ct}$  showed a strong temperature dependence as shown in Figures S8a and b. Based on these results, the activation energy ( $E_a$ ) is calculated.

Figures S8c and d show a linear relationship between the interfacial  $R_{ct}$  and absolute temperature based on the potential and temperature dependences of the values of  $R_{ct}$ .  $E_a$  was evaluated, which can provide quite accurate information on the interfacial lithium transfer, using the plots in Figure S8c and d and Arrhenius equation as follows:<sup>1-3</sup>

$$\frac{1}{R_{ct}} = A \exp\left(-\frac{E_a}{RT}\right) \quad (1)$$

where  $T$  is the absolute temperature,  $R$  is the universal gas constant, and  $A$  is the frequency factor. The electrode was charged to an oxidation potential (for NCM622 thin-film: 3.80 V, NCM622-SSOL thin-film: 3.85 V), at which the cell was kept for sufficient times to reach the kinetic balance before the EIS analysis. The values of  $E_a$  at NCM622 thin-film and NCM622-SSOL thin-film electrodes were estimated to be 54–58 and 49–51 kJ mol<sup>-1</sup>, respectively. The value at the NCM622-SSOL thin-film was lower than that at the NCM622 thin-film electrode, implying that the energy barrier for the lithium transfer at the interface between NCM622-SSOL thin-film and electrolyte was smaller than that at NCM622-bare thin-film electrode. In our previous works, it has been demonstrated that the surface modification can decrease the value of  $E_a$  during charge transfer process in lithium layered oxide electrode/organic electrolyte systems.<sup>4,5</sup> If the rate determining step of the charge transfer reaction depends on the ion transfer reaction rather than the electron transfer, related to the enough electron conductivity of the material, it is considered that the decrease of the value of  $E_a$  for the charge transfer reaction is probably caused by some interactions between modification surface and lithium-ions. Although precise mechanism cannot be clarified in this study, it should be described that the SSOL phase affect not only the surficial stabilization but also the kinetics of charge transfer reaction, which is consistent with the results of CV and  $dQ/dV$  vs.  $V$ .

### **S1.2. XPS spectra of O 1s of NCM622-bare and NCM622-SSOL thin-film electrodes after electrochemical cycles**

The core-level O 1s spectra of NCM622-bare and NCM622-SSOL thin-film electrodes after 30 cycles are displayed in Figure S9 and the fitting results are

summarized in Table S3. The results revealed that the NCM622-bare thin-film electrode had a much higher defect ratio at the surface than that at the NCM622-SSOL thin-film electrode. It is suggested that the spinel-like derivate phase induced by the oxygen vacancy largely exists at the surface of the NCM622 thin-film, which can trigger the formation of the disordered amorphous structure and other derivative phases.<sup>6,7</sup> However, this decay was restrained by combining with SSOL phase on the surface, which was identical to the HR-TEM images in Figure 5.

#### References:

- (1) Nakayama, N.; Nozawa, T.; Iriyama, Y.; Abe, T.; Ogumi, Z.; Kikuchi, K. Interfacial lithium-ion transfer at the  $\text{LiMn}_2\text{O}_4$  thin film electrode/aqueous solution interface. *J. Power Sources* **2007**, *174*(2), 695–700.
- (2) Yamada, Y.; Iriyama, Y.; Abe, T.; Ogumi, Z. Kinetics of Electrochemical Insertion and Extraction of Lithium Ion at  $\text{SiO}_2$ . *J. Electrochem. Soc.* **2010**, *157*(1), A26.
- (3) Yamada, Y.; Iriyama, Y.; Abe, T.; Ogumi, Z. Kinetics of lithium ion transfer at the interface between graphite and liquid electrolytes: effects of solvent and surface film. *Langmuir* **2009**, *25*(21), 12766–70.

(4) Iriyama, Y.; Kurita, H.; Yamada, I.; Abe, T.; Ogumi, Z. Effects of surface modification by MgO on interfacial reactions of lithium cobalt oxide thin film electrode. *J. Power Sources* **2004**, *137*(1), 111–116.

(5) Oriyasa, Y.; Takamatsu, D.; Yamamoto, K.; Koyama, Y.; Mori, S.; Masese, T.; Mori, T.; Minato, T.; Tanida, H.; Uruga, T.; Ogumi, Z.; Uchimoto, Y. Origin of Surface Coating Effect for MgO on LiCoO<sub>2</sub> to Improve the Interfacial Reaction between Electrode and Electrolyte. *Adv. Mater. Interfaces* **2014**, *1*(9), 1400195.

(6) Jung, S.-K.; Gwon, H.; Hong, J.; Park, K.-Y.; Seo, D.-H.; Kim, H.; Hyun, J.; Yang, W.; Kang, K. Understanding the Degradation Mechanisms of LiNi<sub>0.5</sub>Co<sub>0.2</sub>Mn<sub>0.3</sub>O<sub>2</sub> Cathode Material in Lithium Ion Batteries. *Adv. Energy Mater.* **2014**, *4*(1), 1300787.

(7) Jung, R.; Metzger, M.; Maglia, F.; Stinner, C.; Gasteiger, H. A. Chemical versus Electrochemical Electrolyte Oxidation on NMC111, NMC622, NMC811, LNMO, and Conductive Carbon. *J. Phys. Chem. Lett.* **2017**, *8*(19), 4820–4825.

S2. Additional Figures:

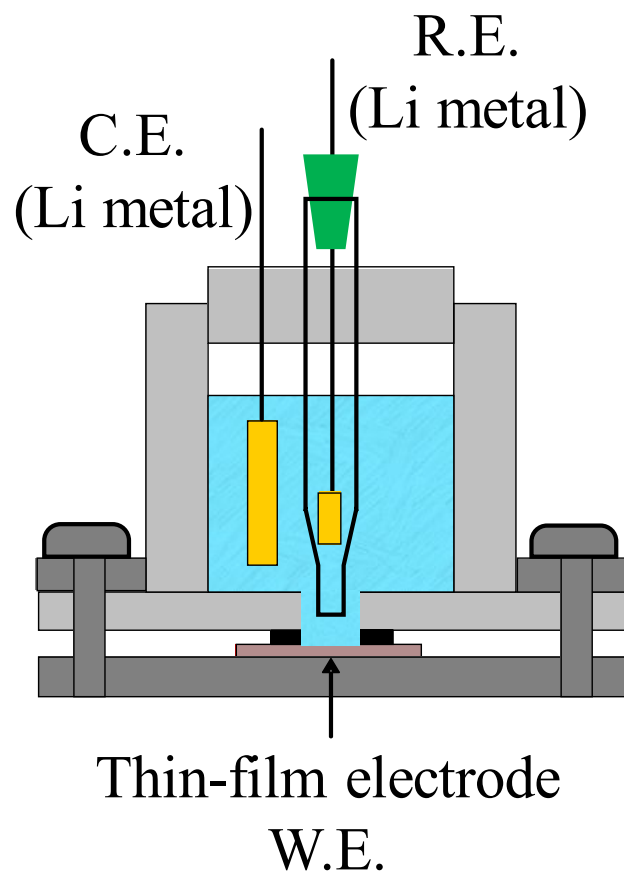
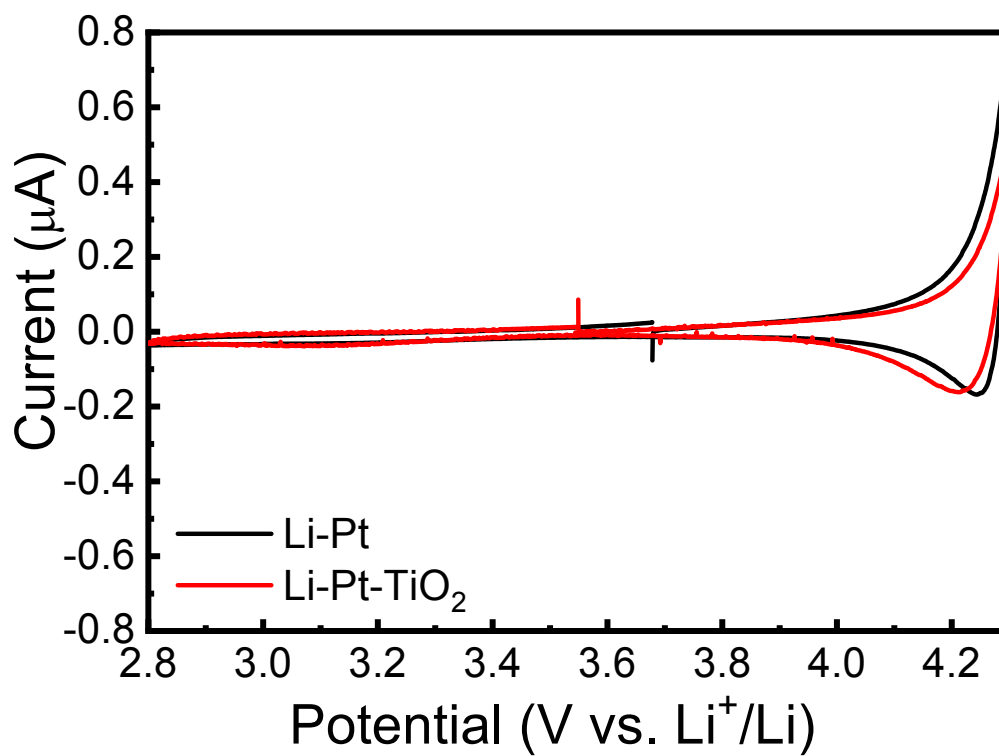
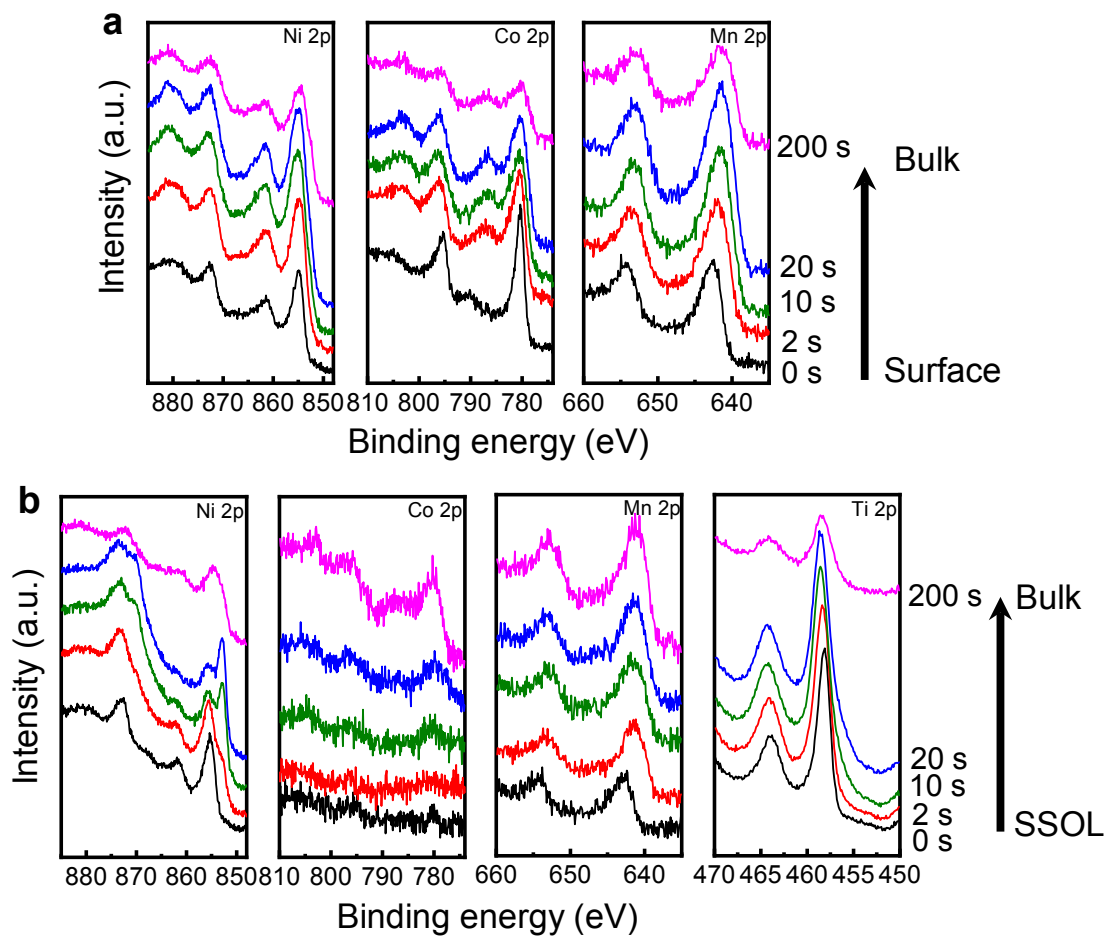


Figure S1. A schematic illustration of a three-electrode cell.



**Figure S2.** CV curves of lithium impurity phases ( $\text{Li}_2\text{PtO}_3$ ) on the Pt substrate under the scan rate of  $0.1 \text{ mV s}^{-1}$ . Pristine electrode only using lithium acetate (black line), after being coated with  $\text{TiO}_2$  (Red line).



**Figure S3.** XPS depth profiling of different detected elements of a) NCM622-bare and b) NCM622-SSOL thin-film electrode before (bottom) and etching for 200 s (upper).

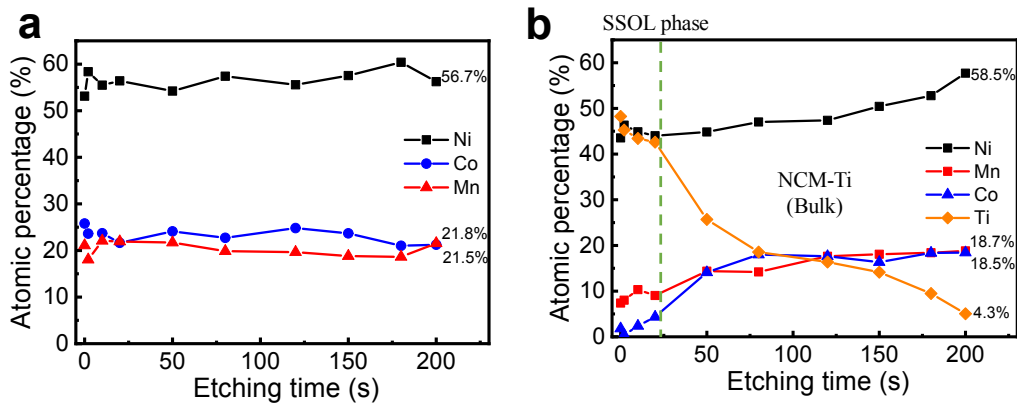


**Figure S4.** Depth profiles from surface to the bulk phase based on XPS spectra etching for 200 s of Ni 2p, Mn 2p, Co 2p, and Ti 2p of a) NCM622-bare and b) NCM622-SSOL thin-film electrodes.

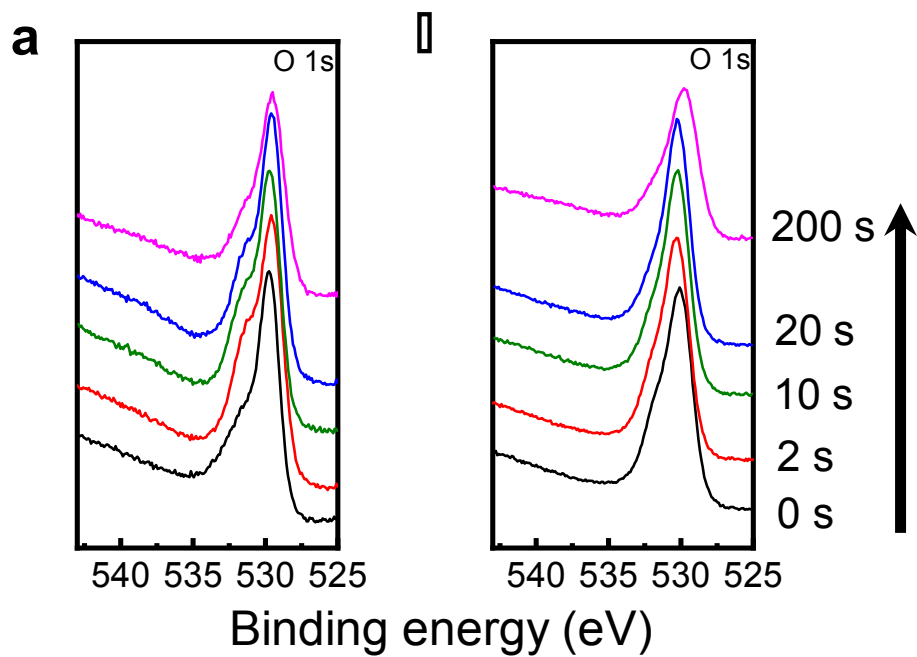


**Figure S5.** XPS depth profiling of O 1s of a) NCM622-bare and b) NCM622-SSOL thin-film electrode before (bottom) and etching for 200 s (upper).

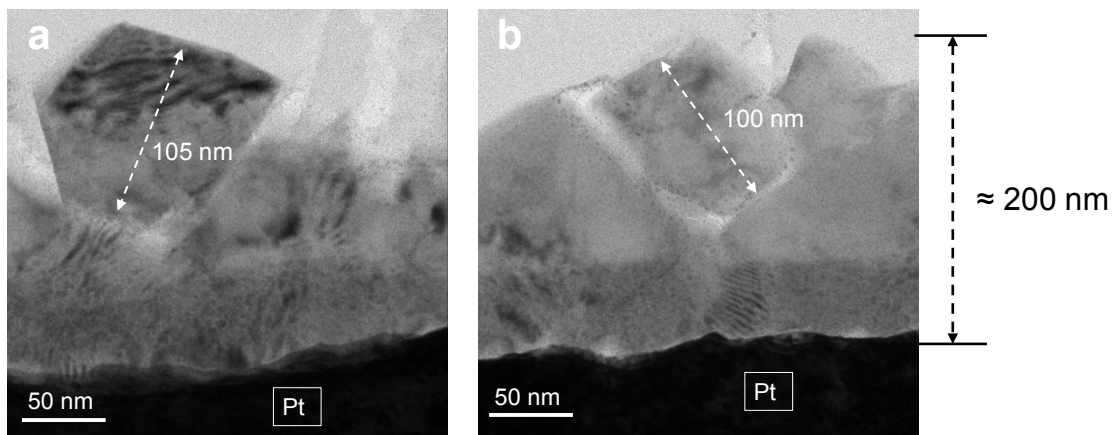


**Figure S6.** Cross-sectioned TEM images a) NCM622-bare and b) NCM622-SSOL thin-film electrodes.

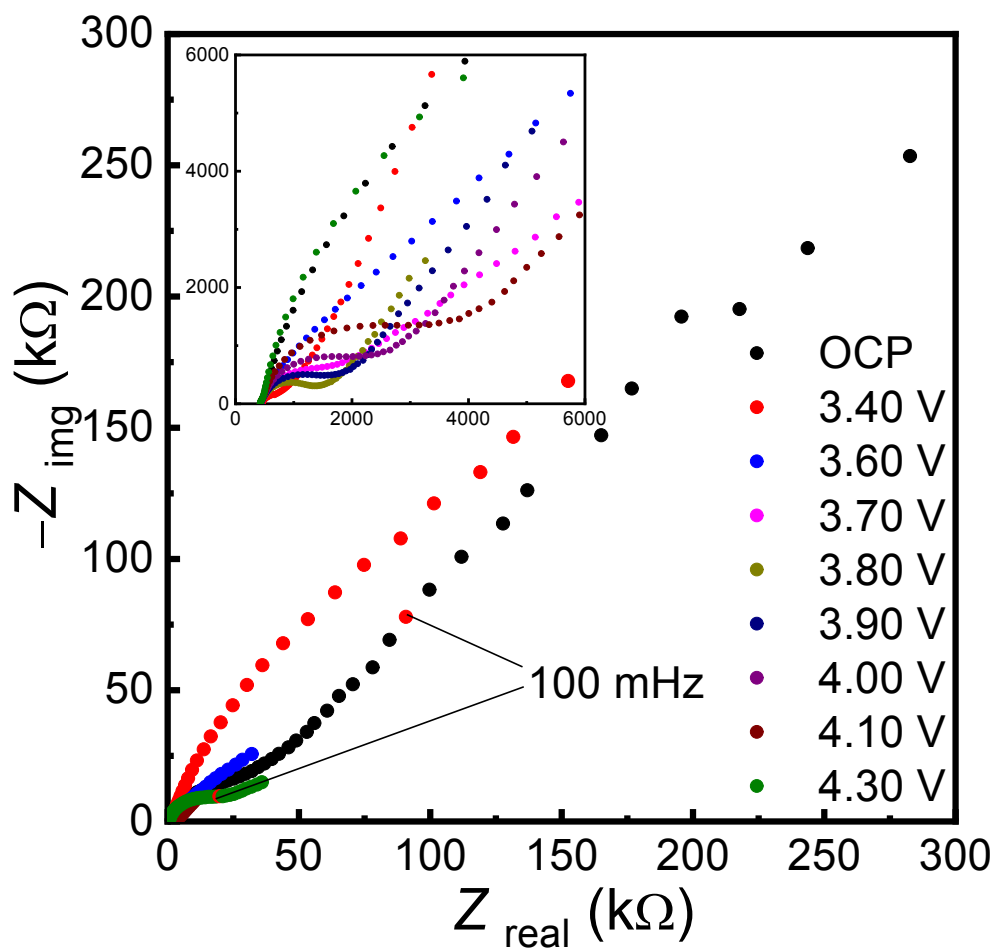


**Figure S7.** Nyquist plots at different potentials during the first charge of a NCM622-bare thin-film electrode.

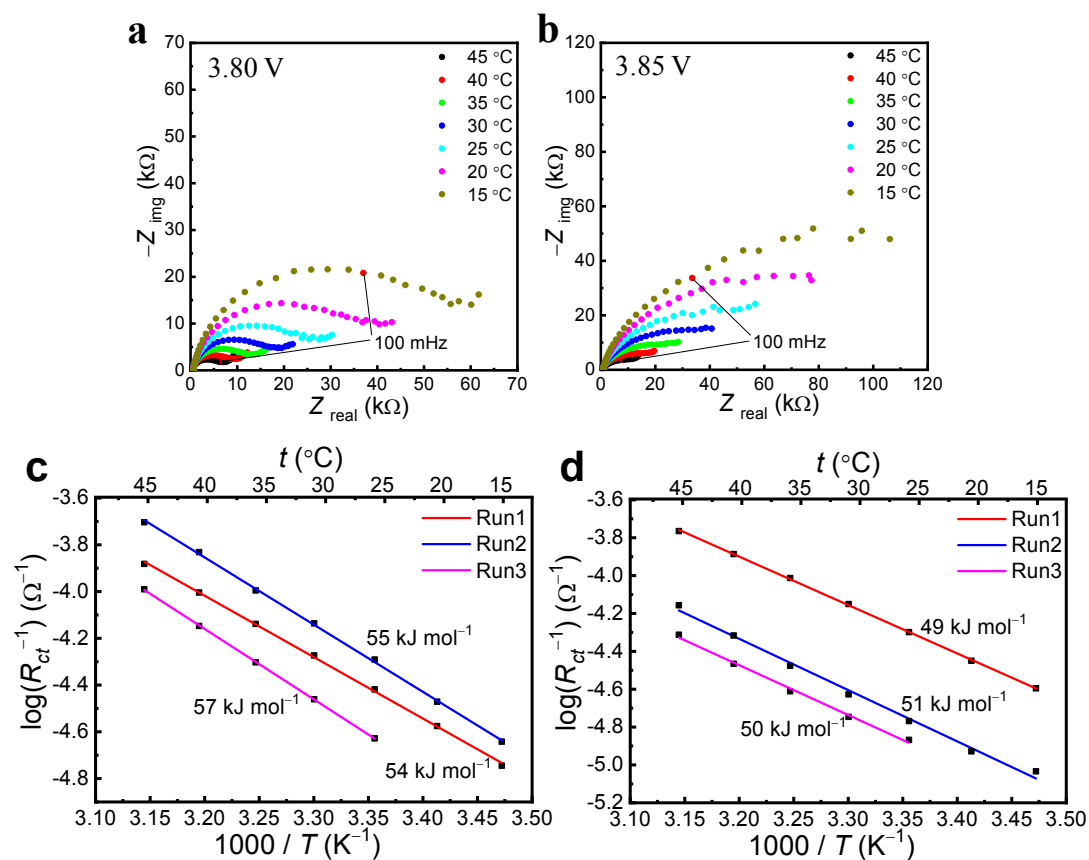


**Figure S8.** The temperature dependences of electrochemical impedance at the main redox  $\log(R_{\text{ct}}^{-1})$  potential of a) NCM622-bare and b) NCM622-SSOL thin-film electrodes. The plots of  $\log(R_{\text{ct}}^{-1})$  against  $1000/T$  of c) NCM622-bare and d) NCM622-SSOL thin-film electrodes for  $E_a$  calculation.

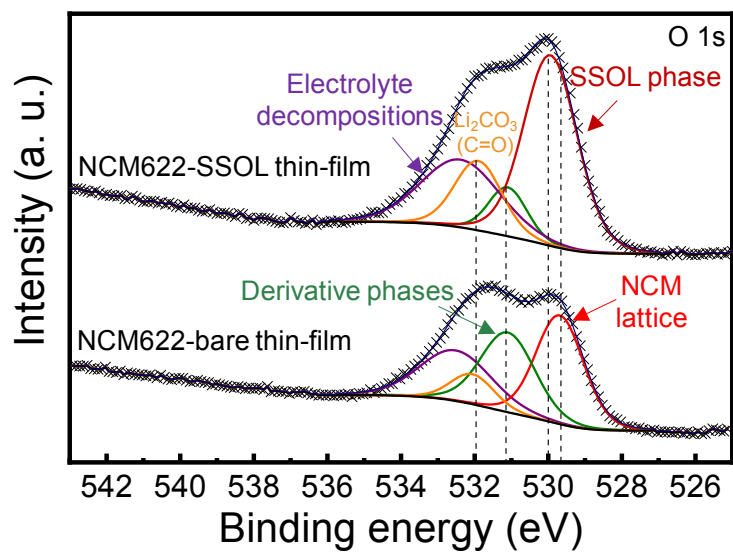


**Figure S9.** XPS spectra of O 1s of NCM622-bare and NCM622-SSOL thin-film electrodes after 30 cycles.

**Table S1.** Chemical concentrations of Ni, Co and Mn for the NCM622 thin-film material detected by ICP-AES

Elements	Chemical concentration (at %)		
	Ni	Co	Mn
Sample			
NCM622 thin-film	60.8	19.7	19.5

**Table S2.** The fitting results of O 1s spectra of NCM622-bare and NCM622-SSOL thin-film electrodes before electrochemical cycles

Samples	Derivatives	NCM lattice	C=O	Defect ratios <sup>a)</sup> (%)
NCM622 thin-film				
Surface (0 s)	31.99	66.5	1.1	32.5
Etching for 50 s	20.68	79.32	–	20.68
NCM622-SSOL thin-film				
Surface (0 s)	12.64	73.86	13.51	14.6
Etching for 50 s	5.4	87.03	7.57	5.8

<sup>a)</sup> Defect ratios: Derivatives / (Derivatives + NCM lattice)

**Table S3.** The fitting results of O 1s spectra of NCM622-bare and NCM622-SSOL thin-film electrodes after 30 cycles

Samples	Derivatives	NCM lattice	Li <sub>2</sub> CO <sub>3</sub> (C=O)	Electrolyte compositions	Defect ratios <sup>a)</sup> (%)
NCM622-bare	29.85	36.11	9	25.04	45.3
NCM622-SSOL	9.04	49.38	15.78	25.81	15.5

<sup>a)</sup> Defect ratios: Derivatives / (Derivatives + NCM lattice)